Available online at www.sciencedirect.com
ScienceDirect
Bioorganic & Medicinal Chemistry 14 (2006) 8420–8429
Bioorganic & Medicinal Chemistry

A platform for designing HIV integrase inhibitors. Part 2: A two-metal binding model as a potential mechanism of HIV integrase inhibitors

Takashi Kawasuji,[a,*] Masahiro Fuji,[a] Tomokazu Yoshinaga,[b] Akihiko Sato,[b] Tamio Fujiwara[b] and Ryuichi Kiyama[a]

[a]*Shionogi Research Laboratories, Shionogi & Company, Ltd, Sagisu, Fukushima-ku, Osaka 553-0002, Japan*
[b]*Shionogi Research Laboratories, Shionogi & Company, Ltd, Mishima, Settsu-shi, Osaka 556-0022, Japan*

Received 21 June 2006; revised 28 August 2006; accepted 29 August 2006
Available online 26 September 2006

Abstract—We propose a two-metal binding model as a potential mechanism of chelating inhibitors against HIV integrase (HIV IN) represented by 2-hydroxy-3-heteroaryl acrylic acids (HHAAs). Potential inhibitors would bind to two metal ions in the active site of HIV IN to prevent human DNA from undergoing the integration reaction. Correlation of the results of metal (Mg^{2+} and Mn^{2+}) titration studies with HIV IN inhibition for a series of active and inactive compounds provides support for the model. Results suggest Mg^{2+} is an essential cofactor for chelating inhibitors.

1. Introduction

Integration of viral DNA into host DNA is an essential step in viral replication of HIV. The integration reaction consists of two distinct stepwise reactions.[1] The first step 3′-processing is a hydrolyzing reaction to remove a terminal dinucleotide to recess a CA-3′ terminal. The CA-3′ sequence is generally conserved on the third and fourth position from both 3′-ends of long terminal repeats of the viral DNA. The second step called strand transfer is a trans-esterification reaction of the recessed 3′-ends with the phosphodiester backbone of the host cell DNA. Both ends of the viral DNA are joined to the host DNA at the same time, and subsequent repair of the nick by host cell repair machinery completes the integration sequence.

HIV IN is composed of three necessary domains:[1] N-terminal (1–50aa), core (51–210aa), and C-terminal (211–288aa) domains. The N-terminal domain has an HHCC motif and shows a zinc finger-like folding with a Zn^{2+} ion. It is thought to affect multimer formation of HIV IN. The C-terminal domain shows an SH-3 like folding and has a non-specific affinity to DNA. A unique active site in the core domain has become an attractive target of molecular biology to understand the mechanism of the integration reaction, and many crystallographic studies have been reported.

HIV IN belongs to a broader class of nucleotide-related enzymes[2] including nucleases, polymerases, and polynucleotidyl transferases. These enzymes commonly have an acidic amino residue cluster in the active sites, which are known to be essential for their native functions. The critical residues are thought to hold metal cofactors, which directly catalyze hydrolysis and/or transesterification reactions of phosphoryl esters of nucleotides according to a two-metal-ion catalysis mechanism.[2]

In the active site of HIV IN, three acidic residues, D64, D116, and E152, the 'catalytic triad,' are conserved among all viral strains. HIV IN is thought to catalyze the two-step integration reaction with two metal ions held by the catalytic triad as illustrated in Scheme 1. The two metal cofactors of HIV IN are thought to be Mg^{2+} under physiological condition.[1]

Mg^{2+} was frequently found to be coordinated by the carboxylic groups of D64 and D116 of the catalytic triad

Keywords: HIV integrase inhibitor; Two-metal binding model; Inhibition mechanism; Docking model; Metal affinity.
* Corresponding author. Fax: +81 6 6458 0987; e-mail: takashi.kawasuji@shionogi.co.jp

0968-0896/$ - see front matter © 2006 Elsevier Ltd. All rights reserved.
doi:10.1016/j.bmc.2006.08.043

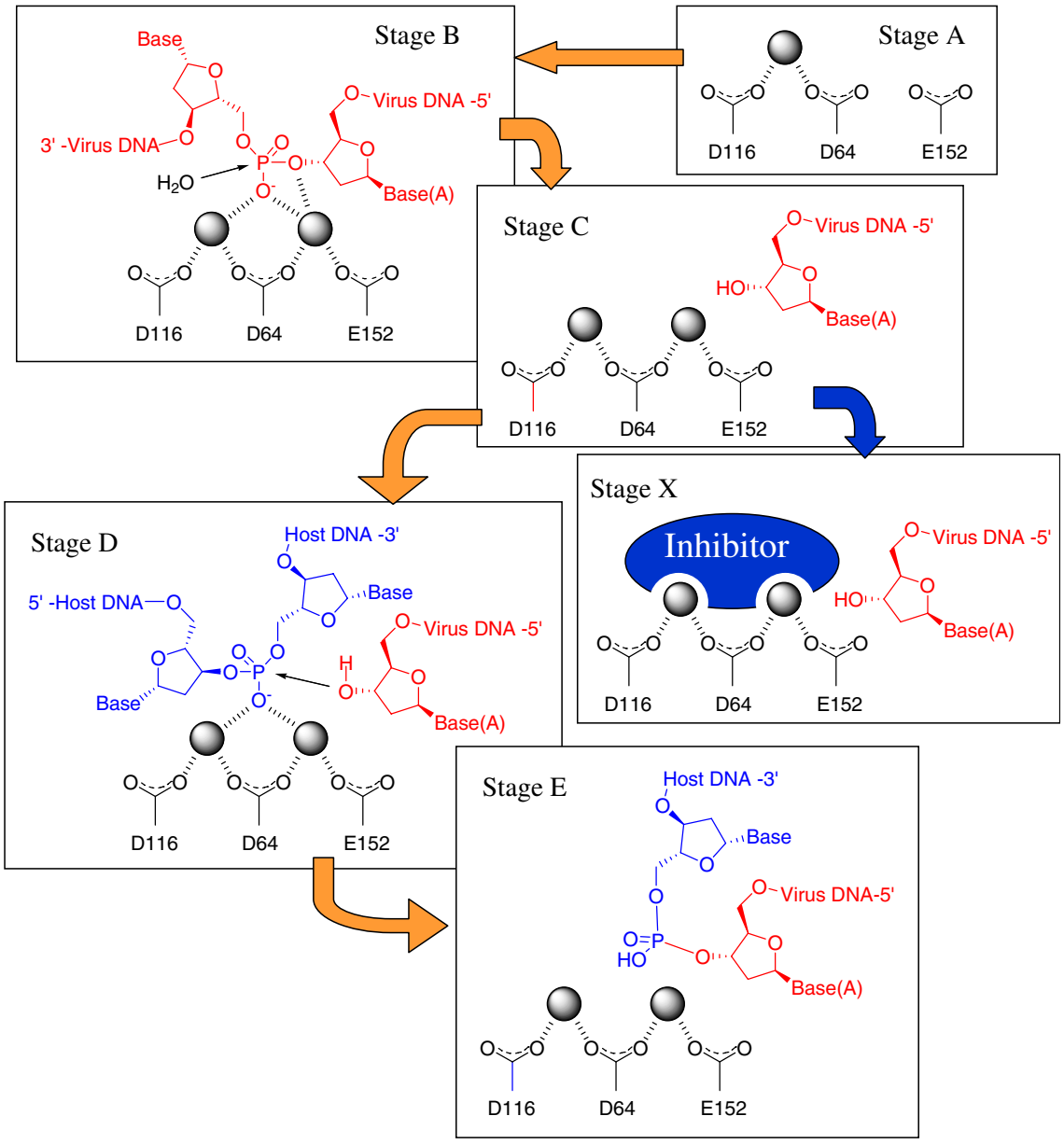

Scheme 1. The two-metal-ion catalysis and inhibition mechanism. Stage A to Stage C indicates the 3′-processing reaction and Stage C to Stage E the strand transfer reaction. (Stage A to B) The enzyme recognizes the adenine base conserved in the third position from 3′-end of viral DNA[1], then activates the next phosphoric ester with the two metals. (Stage B to C) The activated phosphoryl ester is hydrolyzed to excise the terminal dinucleotide and the recognized adenosine is exposed as the new 3′-end, giving a pre-integration complex.[1] (Stage C to D) The pre-integration complex non-specifically[1] binds to host DNA to activate a phosphoryl ester by the two metals. (Stage D to E) The activated phosphoric ester is attacked by the recessed 3′-end in the manner of S_N2-like nucleophilic reaction,[1] then the viral DNA and the host DNA are joined with each other. (Stage X) An inhibitor chelates to the two metal ions of Stage C to block the host DNA binding.

in crystal structures of the HIV IN core domain (Fig. 1a). No another metal ions were reported in crystal structures of HIV IN in the Protein Data Bank,[3] however, two Zn^{2+} or Cd^{2+} were detected in a core domain of ASV IN (avian sarcoma virus integrase).[4] ASV IN core domain exhibits high sequential and functional homology with the HIV IN core domain (Fig. 1a). In ASV IN, one metal is coordinated by the carboxylic groups of D64 and D121 with a similar coordination geometry to that observed in the HIV IN cocrystal structure with a Mg^{2+} (1biu.pdb, 1qs4.pdb). The other Mg^{2+} is coordinated by D64 and E157. Each of the carboxylic oxygens of D64 is coordinating with a different metal ion. Two metal ions are 3.6 Å apart and surrounded by water molecules. Such a complex of zinc or cadmium would be artificial only in the crystallization buffer condition because it does not promote a complete enzymatic reaction.[4] The coordinates of the active site presumably represent the structure that catalyzes the integration reaction, and possibly become a primary template to construct a relevant active site model of HIV IN. Preliminary modeling work was performed starting from the co-crystal structure[5] of HIV IN with a Mg^{2+} (1biu.pdb). Only rotating torsion angles of the E152 residue and an

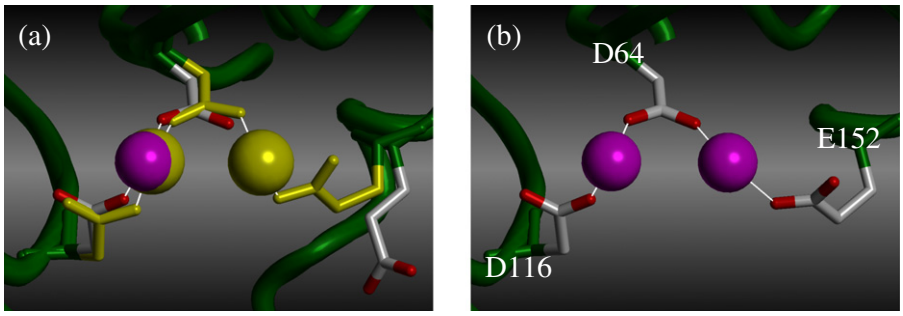

Figure 1. Modeling of HIV IN active site with two magnesium ions. (a) Superimposed model of the template and the starting material based on Cα positions of each catalytic triad (ASV IN: D64, D121, E157. HIV IN: D64, D116, E152). Template: ASV IN active site with two Zn^{2+} (1vsh.pdb). Zn^{2+} are represented as yellow spheres, and the catalytic triad by yellow sticks. White lines indicate coordination of the carboxylic oxygen to the metal ion. Starting material: HIV IN active site with a Mg^{2+} (1biu.pdb). Mg^{2+} is represented as a magenta sphere, and the catalytic triad by stick model colored by atom type. (b) A relevant model of HIV IN active site with two Mg^{2+}, achieved by torsional rearrangement of E152 side chain and the additional metal ion.

extra magnesium ion were sufficient to be compared to the active site of ASV IN as shown in Figure 1b. The Mg^{2+} from the starting material is coordinated by D64 and D116, and the additional ion by D64 and E152. Each of the carboxylic oxygens of D64 is coordinating to different metal ions with a distance of 3.6 Å. The active site exposes two Mg^{2+} on its surface for access to DNA.

We previously reported 2-hydroxy 3-heteroaryl acrylic acid derivatives (HHAAs) as potential inhibitors against HIV IN.[6] The general structure is composed of a substituted heteroaromatic ring 'Prime-Ring' and a 2-hydroxy acrylic acid substructure (HAA), represented by three compounds with characteristic hydrophobic substituents (Fig. 2a). Modeling studies of the three compounds identified 'the most favorable benzene (MFB) space' where the terminal phenyl ring should occupy as shown in Figures 2b and c. Also the carboxylic acid, the enolic hydroxyl group, and the common nitrogen atom in the Prime-Ring were found to be essential for inhibitor activity. Finally we produced the pharmacophore model which is composed of the three hydrophilic functional groups and the MFB space.

We propose a two-metal binding model[7] as a potential inhibition mechanism of HHAAs against HIV IN. An inhibitor chelates to the two metal ions at Stage C to block access of a host DNA to the integrase enzyme as shown in Stage X in Scheme 1. Inhibition of HIV IN can also occur through Stage A however, the HHAAs being strand transfer selective inhibitors as has been shown for the related DKAs.[8] A potential reason that only one Mg^{2+} has been detected in the active site in crystallographic studies is that binding of the viral DNA might be critical for stability of the second metal binding and thus a more realistic representation of actual physiological conditions. The inhibitors would need both metal ions to bind strongly. A series of modeling studies were performed using the typical HHAAs as test ligands to construct a binding model based on this hypothesis. This inhibition model was compared with the structure–activity relationships (SARs) and metal titration studies of HHAAs.

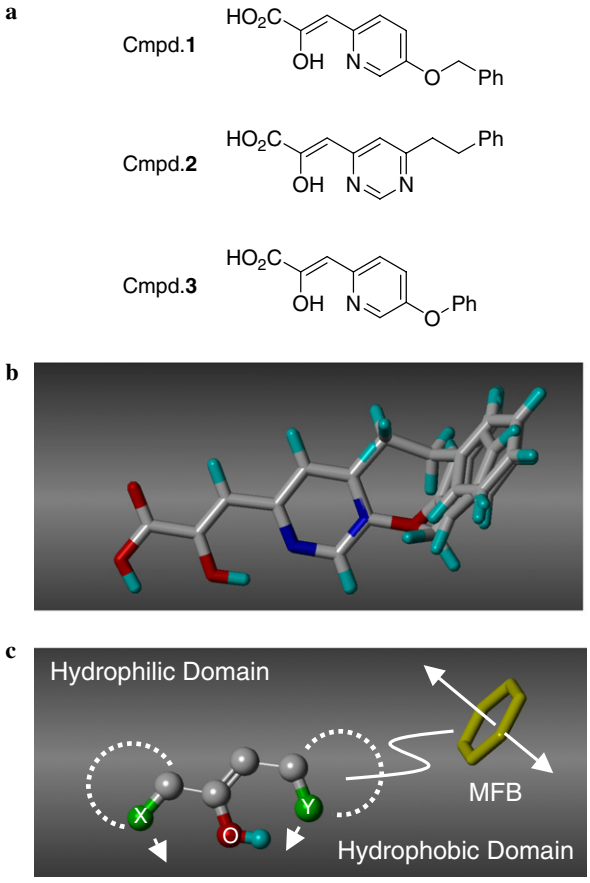

Figure 2. Pharmacophore model for HIV IN inhibitors. (a) Potent inhibitors representing different types of HHAAs. (b) The inhibitors are superimposed based on the hydrophilic region, and every terminal phenyl rings occupy an identical space. (c) The pharmacophore model consists of the hydrophilic and the hydrophobic features. The atoms 'X' and 'Y' represent possible hetero-atoms that serve a lone-pair indicated by white arrows. The yellow hexagon labeled MFB (the most favorable benzene) indicates the average space of all terminal phenyl rings in the superimposed model. The arrow passing through the MFB indicates a favorable direction of the ring plane. The semicircles written in broken line indicate heteroaromatic rings optionally including the 'C=X' or 'C=Y' bond. Two bonds connecting three hydrophilic functional groups are possible to rotate. The winding line indicates a possible linker to connect the hydrophilic domain and a terminal phenyl ring.

The original concept of the two-metal binding model was disclosed in a patent application by our group in 2001.[7] Subsequently, others have published similar ideas to present not only an inhibition mechanism against HIV IN but also a potential strategy[9] to design novel inhibitors of several nucleotide-related enzymes working with two metal cofactors. In brief, new inhibitors can be designed as a possible two-metal chelating scaffold with appropriate substituents for each target molecule. Recently a general inhibition model of DKAs and some chelatable agents against influenza endonuclease was reported by Parkes.[10] Herein we present a modeling study of the two-metal inhibition model of the HHAAs, with additional SAR information around the HHAAs.

2. Chemistry

A selective benzyl extension on the methyl group of compound **4**[6] was achieved by deprotonation and alkylation with benzyl bromide resulting in formation of compound **5** (Scheme 2). The condensation reaction was performed with excess di-*tert*-butyl oxalate under anhydrous conditions to give the corresponding ester **6**. Hydrolysis using trifluoroacetic acid served to provide compound **7**. The corresponding ethyl ester of compound **6** derived from compound **5** and diethyl oxalate was not useful since attempts at basic hydrolysis resulted in complete cleavage back to compound **5**. Compounds **9** and **10** were prepared from compound **8**[6] by aminolysis under refluxing conditions. Compound **12** was obtained from compound **11**[6] by amide coupling.

3. Results and discussion

The hydrophilic pharmacophore region with two metal ions shows a 5,6-bicyclic chelating system, as shown in Figure 3. The hydrophilic region is composed of substructure A and B, known to be bidentate chelatable fragments making a five-membered and a six-membered coordinating system, respectively. In this case, the middle hydroxyl group should be easily ionizable resulting in a formal negative charge enhancing its ability to coordinate to both metal ions at the same time. This is in agreement with the fact that a reduction of the enolic group to the corresponding secondary alcohol gave a complete loss of activity as reported.[6] Although an alternate keto form can serve two lone-pairs to coordinate to the two metals, the neutral molecule is unlikely to chelate strongly. It should be noted that the proposed coordinating system is represented in the cocrystal structure of 4-(1′-carbonyl-2′-oxopropylidene)-2,2,5,5-tetramethyl-3- imidazolidine-1-oxyl with divalent copper ion (Fig. 4).[11] In brief, two 5,6-parallel chelating systems are constructed with two ligands and two copper ions 4 Å apart from each other.

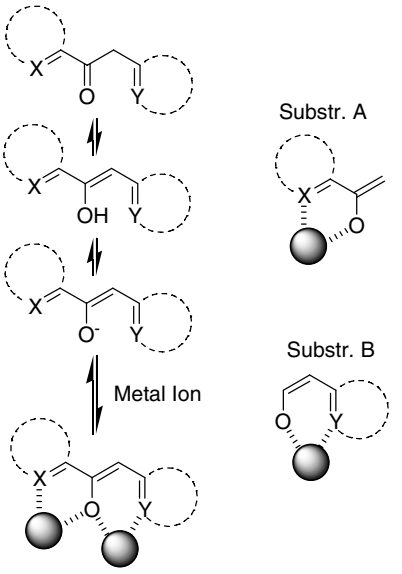

Figure 3. The hydrophilic pharmacophore with two-metal ions. The equilibrium indicates translations from/to each localized form of keto, enol, enolate anion, and two metal chelating state. Substructures A and B pictorially represent each bidentate chelating manner.

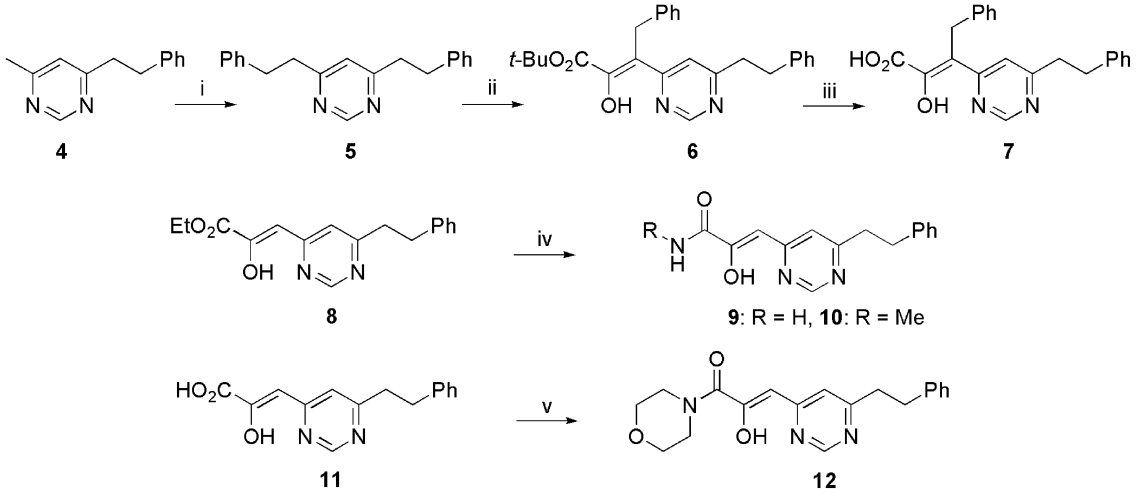

Scheme 2. Preparations of HHAA and amide derivatives. Reagents and conditions: (i) *n*-BuLi, benzylbromide/THF −78 °C; (ii) *n*-BuLi, $(CO_2$-*tert*-$Bu)_2$/THF −78 to 0 °C; (iii) TFA/CH_2Cl_2 rt; (iv) methylamine or ammonia, AcOH/EtOH, reflux; (v) PyBOP, morpholine, HOBt/THF, rt.

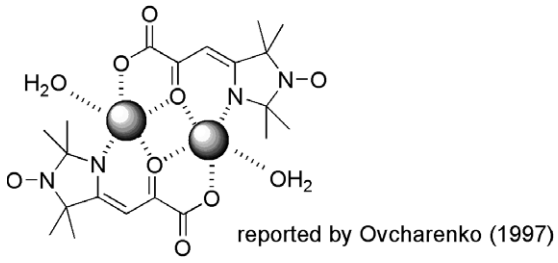

Figure 4. The known crystal structure of two-metal chelating state. It represents a five-membered and a six-membered chelating system partially overlapping with each other. Two Cu^{2+}, two water molecules, and two main molecules are observed in an asymmetric unit.

Figure 5a represents a structural model of the 5,6-parallel chelating system consisting of a chelating region of HHAAs and two divalent magnesium ions. Both of the five- and six-membered coordinating systems were structurally optimized to be completely planar and flush with each other. The distance between the two magnesium ions represents 3.6 Å.

The distances between two metal ions in the ligand model are almost identical to that in the HIV IN model described above. This suggested to us that active inhibitors might bind to the two metals in the active site. Our docking approach was simple, docking the ligand model into the protein model so as both metal pairs overlap with each other. Figures 5c and d show a binding model that best achieves tetrahedral-like coordination in both chelating systems. An alternative reversed direction mode, which is not shown in the figure, can be modeled with similar coordinating systems.

3.1. Metal titration studies

The two-metal inhibition model can directly elucidate why compounds **13**–**15**[6] were inactive (Fig. 6). Every heteroatom in the pharmacophore would be indispensable to chelate to the two metal ions. Mutated compounds **13** and **15** have ability to chelate to only one metal ion whereas compound **14** is unable to chelate. These results are supported by following metal titration studies using Mg^{2+} ranging 0 to 3.6 mol/L in the aqueous condition. Figures 6c and e show simple change of UV absorption curves by metal chelation for each of compounds **13** and **15** as indicated by the arrow. No shift was observed for compound **14**. On the contrary, the original compound **2** showed an interesting two-step shift. As indicated by arrows in Figure 6a raising the metal concentration, first induces a change in absorption around 380 nm, followed by the top of the curve shifting toward shorter a wavelength around 340 nm. It could not strictly demonstrate the generation of the 5,6-parallel chelating system, but might indicate participation of the three functional groups in metal coordination in the final status observed at higher metal concentration. It was not observed for one-metal chelating agents **13** and **15** even at high metal concentration.

Other metal ions were investigated to see if they show the same results. Though no shifts of UV absorption

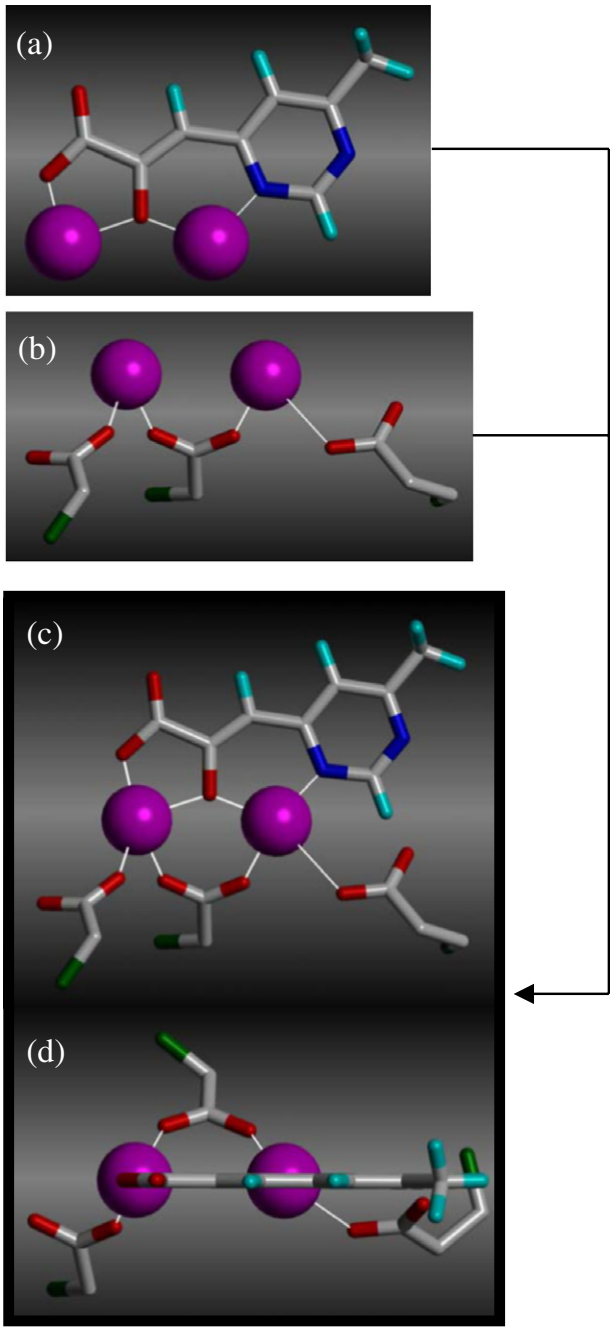

Figure 5. A docking mode of the inhibitor, and the formation of coordinating systems. (a) The graphic shows an optimized model of a HHAA's hydrophilic domain with two Mg^{2+}. (b) Side chains of the catalytic triad and two Mg^{2+} extracted from the protein model. A view from the bottom of Figure 1b. (c) A model of the ligand binding to the two metal ions. (d) A view from the top of (c). Magenta spheres and white lines indicate Mg^{2+} and coordination bonds, respectively.

curves were found using monovalent ions Na^{+} and K^{+}, divalent metal ions Ca^{2+} and Mn^{2+} showed two-step shifts. Ca^{2+} gave a similar shift to that of Mg^{2+} whereas Mn^{2+} did not. It should be emphasized that 50 mM Mn^{2+} is sufficient to find the second shift indicating generation of the last component, even 500 mM is not enough as yet in the case of Mg^{2+}. This indicates that Mg^{2+} needs higher concentration than Mn^{2+} to

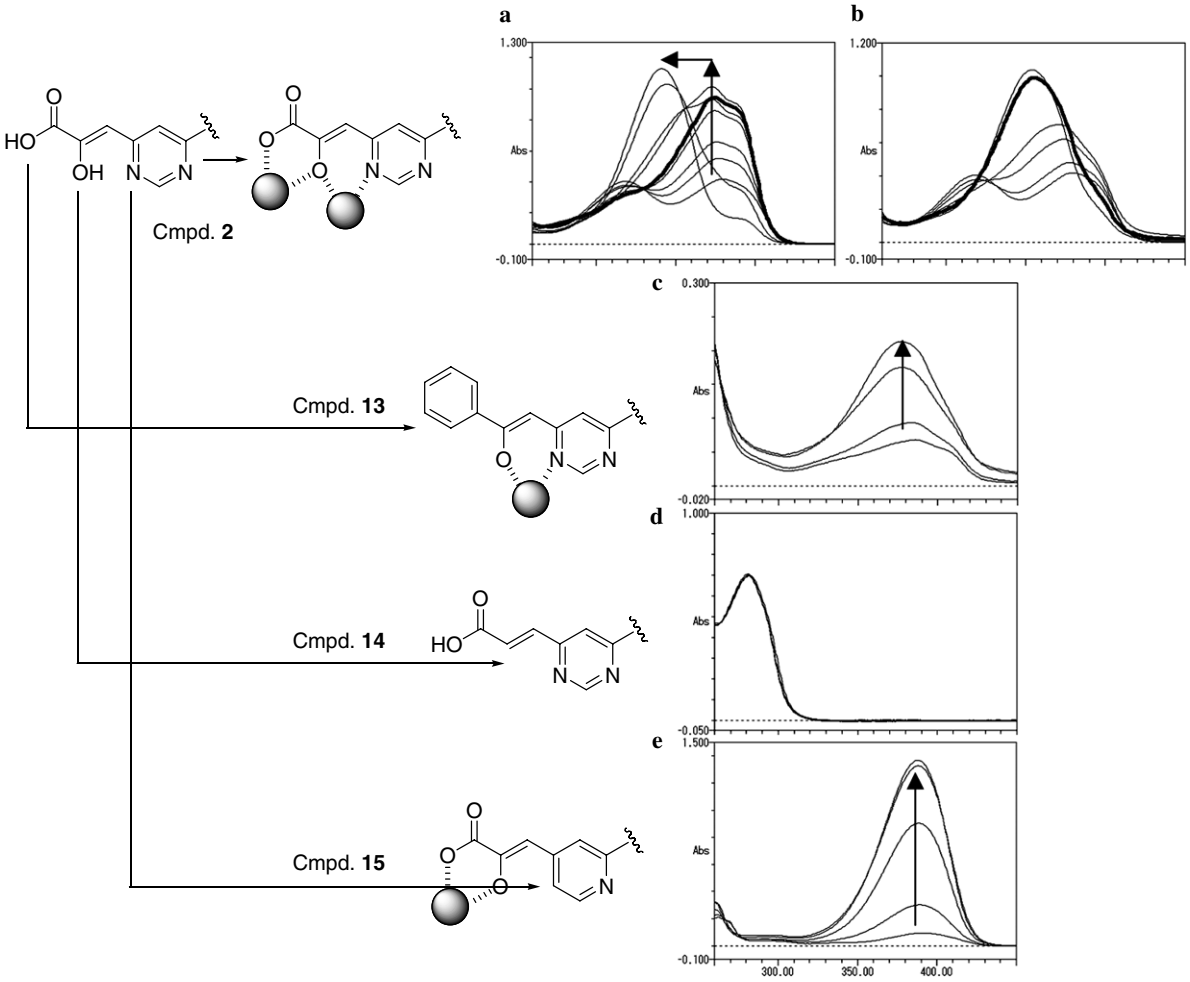

Figure 6. Relationship between potential chelating states and the observation from metal titration studies. The gray spheres indicate metal ions. The pictorial structures of compounds **13**–**15** indicate each potential chelating state. The bending arrows emphasize the mutated position in comparison with model compound **2**. (a and b) The UV spectrum changes of compound **2** by the titration of Mg^{2+} and Mn^{2+}, respectively. The bold curve in (a) indicates the spectrum at 500 mM Mg^{2+}. The bold curve in (b) at 50 mM of Mg^{2+}. (c–e) The UV spectrum changes of each mutated compound by the titration of Mg^{2+}. Arrows in the chart indicate directions of the absorption curve's shift depend on concentration of the metal ion.

generate the final state, or compound **2** is likely to chelate to Mg^{2+} less than Mn^{2+}. Compound **2** showed high potential activity in the MWPA-Mn enzymatic assay using Mn^{2+} as a cofactor, but shows 2 orders of magnitude lower activity in the MWPA-Mg using Mg^{2+} for the replacement of Mn^{2+} as shown in Table 1. The correlation between the inhibitory activity reduction and the metal affinity reduction indicates that the inhibitor directly interacts with metal ions in the active site of HIV IN. Compounds **1** and **3** are representing the different types of HHAAs, showed a similar reduction of activity in the MWPA-Mg, and must show a similar reduction of metal affinity. Among the monovalent and divalent metal cations, only Mn^{2+} and Mg^{2+} are known to promote total enzymatic function in vitro. It should be noticed that antiviral activities in Table 1 are slightly correlated with MWPA-Mg but not MWPA-Mn. Compounds **2**, **3**, **9**, and **10** show moderate activities in both MWPA-Mg and anti-HIV assays, however these are ranging over 3 orders of magnitude in MWPA-Mn. The correlation with MWPA-Mg may provide an experimental support of the generally accepted opinion that Mg^{2+} is the physiological cofactor because of its dominant concentration in cells.[5] Finally it can be suggested that the deficient affinity to Mg^{2+} represents a possible reason of insufficient antiviral activities of HHAAs.

Table 1. Inhibitory activities of each compound in enzymatic and cellular assay

Compound	MWPA-Mn[a] (μM)	MWPA-Mg[b] (μM)	MTT EC_{50}[c] (μM)
1	0.059	2.2	4.8
2	0.037	9.6	34
3	0.37	12	78
7	>277	277	>55
9	71	6.7	49
10	39	11	24
12	262	236	>59

[a,b] Inhibitory activities against the strand transfer. Different metal cofactors were used for each method.
[c] Anti-HIV activities.

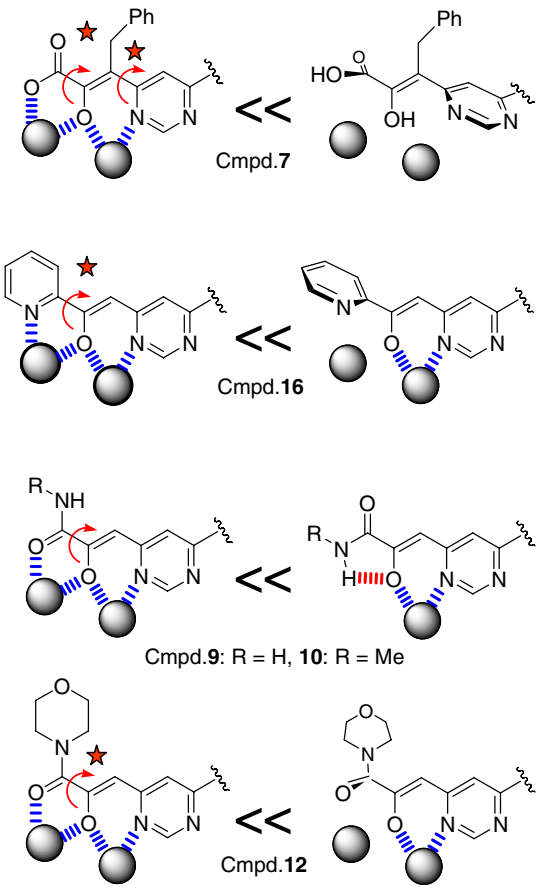

Figure 7. Explanations of why the compounds do not show potential activity. This is to illustrate observations in molecular modeling for the compounds. Sign of inequality indicates likelihood of the conformational change. The red star is attached around the site where the unfavorable intramolecular repulsion can be observed. The blue broken line means coordination to a metal ion represented as a gray sphere, the red broken line is an intramolecular hydrogen bonding. The red curved arrow indicates the bond which would be rotated by an unfavorable intramolecular repulsion or hydrogen bonding.

3.2. Other SARs of HHAAs

Compounds **7**, **9**, **10**, and **12** listed in Figure 7 completely agree with the hydrophilic and hydrophobic pharmacophore summarized in Figure 2, but these were nevertheless inactive in enzymatic assay (MWPA-Mn, Mg) as shown in Table 1. Those contradictions can be clearly explained by the two-metal inhibition model. The model gives additional rules as follows: (1) Every coordinating hetero-atom to serve a lone-pair should be arranged to face the same way to chelate the adjoining two metal ions. (2) A chelating region of an inhibitor should be planar to point each lone-pair toward the metal ions. The extra benzyl group of compound **7** induces serious intramolecular repulsion and consequently warps the chelating region. A 'N–H' group of the carbamoyl and the methyl carbamoyl derivatives **9** and **10** makes unfavorable intramolecular hydrogen bonding with the enolic oxygen and consequently let the amide oxygen face away from the metal ion. Also, the 'N–H' group is not acidic enough to serve as a Lewis base ligand. Though the morpholyl amide derivative **12** does not have such a hydrogen bonding donor, a methylene next to the amide nitrogen makes an unfavorable intramolecular repulsion, giving a contortion of the plane. The 2-pyridyl derivative **16** shows some reduction of inhibitory activity in comparison to 2-pyrimidyl one.[6] The carbon–hydrogen unit for the replacement of the nitrogen atom of the 2-pyrimidyl moiety makes a small intramolecular repulsion as depicted in Figure 7. This discussion does not contradict a potential reason for the activity loss due to extra volume of the benzyl or the morpholyl group.

4. Conclusions

Figure 8 shows one possible docking model of three compounds **1**–**3** representing different types of HHAAs

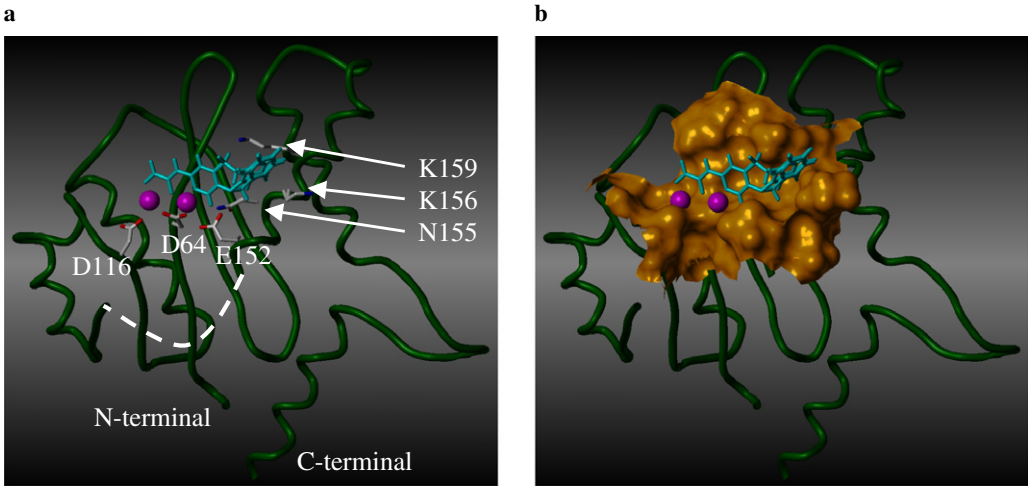

Figure 8. A docking model of HHAAs with IN core domain. (a) IN core domain is represented by a green tube. Side chains of the catalytic triad are shown by stick representation as labeled. Magenta spheres indicate Mg^{2+}. The molecules represented by cyan sticks indicate the active conformers of three compounds **1**–**3** overlapped with each other. The white dotted line indicates a flexible loop (140–149aa) blank in coordinate data. (b) With a Connolly surface around the active site.

in the active site. Those compounds are reproducing each active conformer (a mirror image of Fig. 2b) and chelate to the two Mg^{2+} held by the catalytic triad of HIV IN in the manner of pseudo-tetrahedral coordination (Figs. 5c and d). The terminal phenyl rings in the docking model are placed close to the hydrophobic region of N155, K156, and K159, and no specific interaction or repulsion of the linkers with the protein can be observed. In brief, there is no contradiction between the MFB space model and the observation from the docking model. It should be emphasized that N155S was previously[12] reported to be a resistant mutant of S-1360, whose terminal phenyl ring can be placed[6] at the MFB space to interact with the hydrophobic region. This assists the plausibility of this docking mode, but does not exclude the other modes and should be investigated further. We will need to consider folding of a flexible loop (140–149aa) close to the active site, folding of other domains, and multimer formation of INs and DNAs.

5. Experimental

5.1. Chemistry

^{1}H NMR spectra were determined at 300 MHz. All reactions were carried out under a nitrogen atmosphere with anhydrous solvents that had been dried over type 4 Å molecular sieves.

5.1.1. 4,6-Diphenethyl-pyrimidine (5). A solution of *n*-BuLi (6.7 mL, 1.50 M in *n*-hexane, 10 mmol) was added to a solution of 4-methyl-6-phenethyl-pyrimidine **4**[6] (1.98 g, 10 mmol) in THF (10 mL) at −78 °C. Then a solution of benzyl bromide (1.71 g, 10 mmol) in THF (2 mL) was added to the mixture at −78 °C. The mixture was diluted with a saturated aqueous solution of NH_4Cl and extracted with EtOAc. The organic layer was washed with water and brine, and dried over $MgSO_4$. The solvent was removed in vacuo, and the precipitate was washed with *n*-hexane to give the product as colorless crystals (1.61 g, 56% yield). ^{1}H NMR ($CDCl_3$) δ 3.01 (s, 8H), 6.84 (d, J = 1.5 Hz, 1H), 7.15–7.30 (m, 10H), 9.08 (d, J = 1.5 Hz, 1H).

5.1.2. 2-Hydroxy-3-(6-phenethyl-pyrimidin-4-yl)-4-phenyl-but-2-enoic acid *tert*-butyl ester (6). A solution of *n*-BuLi (2.0 mL, 1.50 M in *n*-hexane, 3 mmol) was added to a solution of compound **5** (865 mg, 3 mmol) in THF (10 mL) at −78 °C. The reaction mixture was stirred for 30 min and then oxalic acid di-*tert*-butyl ester (3.0 g, 15 mmol) was added in one portion. The mixture was then warmed to 0 °C and stirred for 30 min. After dilution with a saturated aqueous solution of NH_4Cl, the mixture was extracted with EtOAc. The organic layer was washed with water and brine, and dried over Na_2SO_4. The solvent was removed in vacuo, then the residue was purified by flash column chromatography using *n*-hexane/EtOAc = 3:1 as eluent to give the product as pale yellow crystals (780 mg, 62% yield). Mp 116–118 °C, ^{1}H NMR ($CDCl_3$) δ 1.47 (s, 9H), 2.91 (s, 4H), 3.79 (s, 2H), 6.69 (d, J = 1.2 Hz, 1H), 7.05 (d, J = 3.0 Hz, 2H), 7.17–7.27 (m, 8H), 8.77 (d, J = 1.2 Hz, 1H).

5.1.3. 2-Hydroxy-3-(6-phenethyl-pyrimidin-4-yl)-4-phenyl-but-2-enoic acid (7). A solution of compound **6** (100 mg, 0.24 mmol) in CH_2Cl_2 (2 mL) and TFA (1 mL) was stirred for 5 h at room temperature. Then the solvent was removed in vacuo, and the precipitate was washed with EtOAc to give the product as pale yellow crystals (80 mg, 92% yield). Mp 188–190 °C, ^{1}H NMR (DMSO-d_6) δ 2.88 (s, 4H), 3.78 (s, 2H), 6.95 (s, 1H), 7.05–7.28 (m, 10H), 8.81 (s, 1H). Anal. Calcd for $C_{22}H_{20}N_2O_3\cdot 0.3H_2O$: C, 72.23; H, 5.68; N, 7.66. Found: C, 72.41; H, 5.47; N, 7.46.

5.1.4. 2-Hydroxy-3-(6-phenethyl-pyrimidin-4-yl)-acrylamide (9). This compound was prepared by a similar method to that described for compound **10**. Yellow crystal, 52% yield. Mp 155–156 °C, ^{1}H NMR ($CDCl_3$) δ 3.00–3.05 (m, 4H), 5.70 (br s, 1H), 6.41 (s, 1H), 6.80 (d, J = 1.2 Hz, 1H), 6.94 (br s, 1H), 7.15–7.35 (m, 5H), 8.83 (d, J = 1.2 Hz, 1H). Anal. Calcd for $C_{15}H_{15}N_3O_2$: C, 66.90; H, 5.61; N, 15.60. Found: C, 66.90; H, 5.62; N, 15.69.

5.1.5. 2-Hydroxy-*N*-methyl-3-(6-phenethyl-pyrimidin-4-yl)-acrylamide (10). A solution of methylamine (1 mL, 30 w/v% in EtOH) was added to a solution of 2-hydroxy-3-(6-phenethyl-pyrimidin-4-yl)-acrylic acid ethyl ester **8**[6] (200 mg, 0.67 mmol) and acetic acid (40 mg, 0.67 mmol) in EtOH (5 mL). The mixture was refluxed for 1 h then the solvent was removed in vacuo. The residue was purified by flash column chromatography using *n*-hexane/EtOAc = 1:1 as eluent to give the product as yellow crystals (50 mg, 26% yield). Mp 155–157 °C, ^{1}H NMR ($CDCl_3$) δ 2.95 (d, J = 5.1 Hz, 3H), 3.05 (s, 4H), 6.41 (s, 1H), 6.79 (s, 1H), 7.06 (s, 1H), 7.15–7.32 (m, 5H), 8.88 (s, 1H). Anal. Calcd for $C_{16}H_{17}N_3O_2\cdot 0.9H_2O$: C, 64.16; H, 6.33; N, 14.03. Found: C, 64.13; H, 6.08; N, 14.18.

5.1.6. 2-Hydroxy-1-morpholin-4-yl-3-(6-phenethyl-pyrimidin-4-yl)-propenone (12). A mixture of 2-hydroxy-3-(6-phenethyl-pyrimidin-4-yl)-acrylic acid **11**[6] (100 mg, 0.37 mmol), PyBOP (420 mg, 0.8 mmol), *N*-methylmorpholine (80 mg, 0.8 mmol), HOBT (110 mg, 0.8 mmol) and morpholine (70 mg, 0.8 mmol) in THF (10 mL) was stirred for 4 h at room temperature. The reaction mixture was diluted with EtOAc, washed with water and a saturated aqueous solution of $NaHCO_3$, then dried over Na_2SO_4. The solvent was removed in vacuo, then the residue was purified by flash column chromatography using EtOAc/MeOH = 20:1 as eluent. Crystallization with *n*-hexane and EtOAc gave the desired compound as yellow crystals (60 mg, 48% yield). Mp 130–132 °C, ^{1}H NMR ($CDCl_3$) δ 2.95–3.10 (m, 4H), 3.65–3.80 (m, 8H), 5.74 (s, 1H), 6.62 (d, J = 1.2 Hz, 1H), 7.18–7.35 (m, 5H), 8.62 (s, 1H). Anal. Calcd for $C_{19}H_{21}N_3O_3\cdot 0.8H_2O$: C, 64.50; H, 6.44; N, 11.88. Found: C, 64.33; H, 6.30; N, 11.88.

5.2. Metal titration studies

UV spectrum data ranging 250–450 nm as wavelength were collected using 1 cm cell. The solution conditions were unified for every measurement as MOPS–NaOH buffer (50 mmol/L, pH 7.4) with 10% DMSO. NaCl was added in exchange for the titrated divalent metal ion to keep the ion strength constant. Compound **2** (50 μmol/L) was titrated by $MgCl_2$ of 0.0, 0.005, 0.01, 0.03, 0.05, 0.5, 1.0, 1.5, 2.0, 3.6 mol/L, or by $MnCl_2$ of 0.0, 0.0005, 0.002, 0.005, 0.05, 0.1 mol/L. Compound **13** (50 μmol/L) was titrated by $MgCl_2$ of 0.0, 0.5, 1.0, 2.0, 3.6 mol/L. Compound **14** (50 μmol/L) was titrated by $MgCl_2$ of 0.0, 0.5, 1.0, 3.6 mol/L. Compound **15** (50 μmol/L) was titrated by $MgCl_2$ of 0.0, 0.005, 0.05, 0.5, 2.0 mol/L.

5.3. Molecular modeling

Modeling studies were performed using the SYBYL 6.9 software package[13] and the WinMOPAC v 2.0 program.[14] Schematic representations of the models were prepared with SYBYL.

5.3.1. Modeling of the ligand model. The 3-D molecular structure of the hydrophilic domain was generated using the Sketch Molecule command of SYBYL. After a relaxation of the hydrophilic domain using the Minimize command, two magnesium atoms were attached to be 2.1 Å from each coordinating atom. The complex was optimized using a semiempirical molecular orbital method with MNDOD Hamiltonian.

5.3.2. Modeling of the preliminary protein model. The atomic coordinates of crystal structures of HIV IN and ASV IN were retrieved from the Protein Data Bank[3] (entry: 1biu.pdb and 1vsh.pdb, respectively). Water molecules were removed from the coordinate sets, giving a primary model of HIV IN and a template model of active site, respectively. The HIV IN model was superimposed over the template model using a rigid-body least-squares fit based on coordinates of Cα of the three acidic amino acid (D64, D116, E152 in HIV IN and D64, D121, E157 in ASV IN). A side chain of the E152 in HIV IN model was fixed by manually rotating to overlap along that of the E157 in the template model. Then an additional magnesium ion was generated in the same position of the zinc ion coordinated by the D64 and E157. Hydrogen atoms were added for whole molecule with standard geometry.

5.3.3. Modeling of the docking model. The ligand model was superimposed into the protein model as both metal pairs overlap with each other by rigid-body manual orientation. The ligand model was oriented to construct a coordinating system that best achieves a tetrahedral-like coordination for both systems. Then the two metals from the ligand model were removed, giving the coordination model shown in Figures 5c and d. Each hydrophobic substituent of active compounds **1**, **2**, and **3** was attached to the ligand with special torsion angles constructing active conformers. Then each of the ligands was superimposed into the coordination model based on the hydrophilic region using the Fit Atoms command of SYBYL, giving the final docking model.

5.4. Assay

Evaluation of inhibitory activities was done by the same method as described in the companion paper.[6] MWPA-Mg enzymatic assay was done with a similar manner to that of MWPA-Mn with a minor modification as the following. Divalent manganese ion was used as a cofactor through all the steps of MWPA-Mn assay. On the contrary, the manganese ion was replaced with divalent magnesium ion after making IN-DNA complex in MWPA-Mg assay, then incubation of a compound and a strand transfer reaction were performed with the same manner of MWPA-Mn assay.

Acknowledgments

The authors thank Prof. Shu Kobayashi for valuable discussions and Dr. Brian A. Johns for assisting with the manuscript preparation.

References and notes

1. For recent reviews on structure and biology of HIV integrase, see: Chiu, T. K.; Davies, D. R. *Curr. Top. Med. Chem.* **2004**, *4*, 965–979.
2. (a) Yang, W.; Steitz, T. A. *Structure* **1995**, *3*, 131–134; (b) Haren, L.; Ton-Hoang, B.; Chandler, M. *Annu. Rev. Microbiol.* **1999**, *53*, 245–281.
3. Bernstein, F. C.; Koetzle, T. F.; Williams, G. J. B.; Meyer, E. F., Jr.; Brice, M. D.; Rodgers, J. R.; Kennard, O.; Shimanouchi, T.; Tasumi, M. *J. Mol. Biol.* **1977**, *112*, 535–542.
4. Bujacz, G.; Alexandratos, J.; Wlodawer, A. *J. Biol. Chem.* **1997**, *272*, 18161–18168.
5. Goldgur, Y.; Dyda, F.; Hickman, A. B.; Jenkins, T. M.; Craigie, R.; Davies, D. R. *Proc. Natl. Acad. Sci. U.S.A.* **1998**, *95*, 9150–9154.
6. Kawasuji, T.; Yoshinaga, T.; Sato, A.; Yodo, M.; Fujiwara, T.; Kiyama, R. *Bioorg. Med. Chem.*, the companion paper, doi:10.1016/j.bmc.2006.08.044.
7. Kiyama, R.; Kawasuji, T. PCT Int. Appl. 2001, WO-01/95905.
8. (a) Hazuda, D. J.; Felock, P.; Witmer, M.; Wolfe, A.; Stillmock, K.; Grobler, J. A.; Espeseth, A.; Gabryelski, L.; Schleif, W.; Blau, C.; Miller, M. D. *Science* **2000**, *287*, 646–650; (b) Espeseth, A. S.; Felock, P.; Wolfe, A.; Witmer, M.; Grobler, J.; Anthony, N.; Egbertson, M.; Melamed, J. Y.; Young, S.; Hamill, T.; Cole, J. L.; Hazuda, D. J. *Proc. Natl. Acad. Sci. U.S.A.* **2000**, *97*, 11244–11249.
9. (a) Grobler, J. A.; Stillmock, K.; Hu, B.; Witmer, M.; Felock, P.; Espeseth, A. S.; Wolfe, A.; Egbertson, M.; Bourgeois, M.; Melamed, J.; Wai, J. S.; Young, S.; Vacca, J.; Hazuda, D. J. *Proc. Natl. Acad. Sci. U.S.A.* **2002**, *99*, 6661–6666; (b) Hazuda, D. J.; Anthony, N. J.; Gomez, R. P.; Jolly, S. M.; Wai, J. S.; Zhuang, L., et al. *Proc. Natl. Acad. Sci. U.S.A.* **2004**, *101*, 11233–11238.
10. Parkes, K. E. B.; Ermert, P.; Fassler, J.; Ives, J.; Martin, J. A.; Merrett, J. H.; Obrecht, D.; Williams, G.; Klumpp, K. *J. Med. Chem.* **2003**, *46*, 1153–1164.

11. Ovcharenko, V. I.; Vostrikova, K. E.; Podoplelov, A. V.; Romanenko, G. V.; Ikorskii, V. N.; Reznikov, V. A. *Polyhedron* **1997**, *16*, 1279–1289.
12. Yoshinaga, T.; Sato, A.; Fujishita, T.; Fujiwara, T. S-1360: In Vitro Activity of a New HIV-1 Integrase Inhibitor in Clinical Development. *Ninth Conference on Retroviruses and Opportunistic Infections*. Seattle, Washington, USA, 24–28 February 2002. Abstracts, 55p, No. 8.
13. SYBYL 6.9; S. Tripos Inc.: St. Louis MO.
14. WinMOPAC v 2.0 program; Fujitsu Ltd: http://www.fujitsu.com.